Applied Catalysis B: Environmental 310 (2022) 121294

Contents lists available at ScienceDirect

Applied Catalysis B: Environmental

journal homepage: www.elsevier.com/locate/apcatb

Aging study of low Ru loading dual function materials (DFM) for combined power plant effluent CO_2 capture and methanation

Chae Jeong-Potter [a], Alessandro Porta [b], Roberto Matarrese [b], Carlo Giorgio Visconti [b], Luca Lietti [b,*], Robert Farrauto [a,*]

[a] Columbia University, Department of Earth and Environmental Engineering, New York 10027, USA
[b] Politecnico Di Milano, Dipartimento di Energia, Milano 20156, Italy

ARTICLE INFO

Keywords:
CCU
CO_2 methanation
DFM stability
Reduced Ru loadings
Simulated power plant effluents

ABSTRACT

This work addresses the stability of different Ru-based dual function materials (DFM, x% Ru, 6.1% "Na_2O"/Al_2O_3) during cycles of CO_2 capture from simulated power plant effluent (320 °C; 7.5% CO_2, 15% steam, 4.5% O_2, balance N_2 (v/v)) and subsequent catalytic methanation. Aging studies are carried out to simulate natural gas combustion flue gas on DFM granules, tablets, and ring tablets prepared by sequentially impregnating Ru and Na_2O. Stability increases with Ru loading; however, 0.5% Ru DFMs demonstrate a small but steady loss of CH_4 produced per cycle consistent with deactivation of the Ru component likely due to exposure to high levels of O_2 and steam in the flue gas. CO chemisorption, in-situ FT-IR, and transient microreactor studies all verify that there is loss in Ru active surface area, possibly due to sintering, which consequently results in lower methanating ability.

1. Introduction

CO_2 average concentration in the atmosphere exceeded 410 ppm in 2019, confirming the steadily increasing levels since the industrial revolution [1]. The detrimental effect of a high concentration of CO_2 in the atmosphere are well known, and international agreements have been put in place to limit anthropic CO_2 emissions. Together with a decrease in the carbon emissions, which can be achieved thanks to the increase in the efficiency of the emitting processes and the shift towards renewable energies, carbon capture and reutilization technologies will play an important role in limiting CO_2 atmospheric concentration [2]. CO_2 can be captured at point sources (e.g., power production facilities, industrial sites) using liquid or solid adsorbent [3]. In both cases the main drawback of the technology is the high amount of energy required to regenerate the adsorbent material. Furthermore, when the adsorbent is regenerated, captured CO_2 is released and needs to be effectively stored or – even better – recycled.

In this context, a possible solution may be provided by dual function materials (DFM) which effectively couple the two steps of carbon capture and utilization [4,5]. These materials act both as solid adsorbents for capture CO_2 and as catalysts for hydrocarbons production from the captured carbon upon H_2 exposure [4]. For this reason, these materials require a carbon capture function (usually an alkaline or alkaline earth metal) and a hydrogenating function (usually Ru) supported on a high surface area carrier [6,7]. In particular, these materials have been developed for CO_2 capture and methanation, envisaging a possible application in cleaning and recycling the carbon content from flue gases of fossil fuel power plants [8,9]. These materials operate in cyclic conditions: first, the material is exposed to the flue gases and saturated with CO_2. The DFM is then exposed to a (renewable) H_2 stream to convert the adsorbed CO_2 to methane (renewable natural gas, RNG). The energy required for the adsorbent regeneration and methanation reaction is supplied by the sensible heat of the flue gases, avoiding the need for external energy inputs. Thus, capture and utilization can be achieved, in principle, with a single material isothermally and isobarically.

To date, the most successful DFM formulation consists of Ru dispersed on γ-Al_2O_3 and doped with "Na_2O" arising from the reduction of Na_2CO_3 [7,9–13]. This combination of catalyst and sorbent has good CO_2 adsorption capacity and fast methanation kinetics [7]. Prior studies have also shown that 5% Ru, 6.1% "Na_2O"/Al_2O_3 DFM tablets were stable for over 50 cycles of capture of CO_2 from flue gas compositions (i.e., N_2, H_2O, CO_2 and O_2) and subsequent conversion to methane at 320 °C and atmospheric pressure [3,12]. Improved performances were even observed on the aged material, linked to slight re-dispersion of the

* Corresponding authors.
E-mail addresses: luca.lietti@polimi.it (L. Lietti), rf2182@columbia.edu (R. Farrauto).

https://doi.org/10.1016/j.apcatb.2022.121294
Received 22 December 2021; Received in revised form 1 March 2022; Accepted 5 March 2022
Available online 31 March 2022

Ru and "Na_2O" [12]. Though a stable material has been identified, economics of 5 wt% Ru (24.1 $/g as of March 2022) can be quite burdensome for wide deployment of this technology and it is beneficial to reduce the cost of materials. To this aim, the stability of low Ru loading DFM (0.5 wt% and 1 wt% Ru) over at least 50 cycles of CO_2 capture and conversion in industrially relevant conditions has been investigated. The DFMs were prepared using Al_2O_3 supports of different shapes (granules, cylindrical tablets, and cylindrical ring tablets) envisioning the use of these materials in a packed bed reactor configuration.

2. Experimental

2.1. Materials preparation

γ-Al_2O_3 (Sasol TH100) was used as support in the form of granules (300 μm diameter, surface area = 148 m^2/g, pore volume = 0.77 cm^3/g), tablets (cylinders, 5 ×5 mm, surface area = 140 m^2/g, pore volume = 0.66 cm^3/g), and ring tablets (cylinders, 5 ×5 mm, with one axial opening of 2 mm diameter, surface area = 139 m^2/g, pore volume = 0.60 cm^3/g). The supports were calcined to 500 °C for 5 h prior to the introduction of the active phases by impregnation. At first, Ru was impregnated using an aqueous solution of ruthenium (III) nitrosyl nitrate ($Ru(NO)(NO_3)_3$) precursor salt (Alfa Aesar, Ru 32 wt%) to obtain a nominal metal loading of 0.5 wt% and 1 wt% Ru. A 10% excess volume with respect to the total pore volume of the support was used during the impregnation in order to favor the uniformity of each catalyst batch. The addition of HNO_3 was required in this step when tablets and ring tablets were used as supports, to achieve homogenous penetration of Ru, according to a previously reported preparation method [14]. Following a similar approach, the amount of HNO_3 (WVR BDH Chemicals, 68%) in the solution was set to a molar ratio of $HNO_3/Ru = 70$ for the 0.5 wt% Ru loading and $HNO_3/Ru = 40$ for the 1 wt% Ru loading. HNO_3 was not added to the Ru impregnating step when DFM were prepared using the granules as the support. All Ru impregnated samples were dried overnight (15 h) in static air at 120 °C.

The dried Ru-impregnated samples were subsequently reduced in H_2 (5 vol% H_2/N_2, 2 L(NTP)/h/g_{DFM}) at 350 °C for 3 h (heating rate: 2 °C/min) to fully decompose the precursor salt and residual HNO_3 possibly remaining on the catalyst after the preparation. The reduced samples were cooled in pure N_2 and passivated at room temperature in a diluted O_2 stream (2 vol% O_2/N_2, 1 L(NTP)/h/g_{DFM}).

An aqueous precursor solution of Na_2CO_3 (Sigma Aldrich, >99%) was impregnated onto the passivated sample in order to obtain a nominal metal loading of 10 wt% Na_2CO_3 (corresponding 6.1 wt% "Na_2O" on the finished DFM weight). A 10% excess of solution with respect to the initial support pore volume was used. The samples were dried using the same procedure as the first impregnation step. The final products are named 0.5% DFM (0.5 wt% Ru, 6.1 wt% "Na_2O"/Al_2O_3) and 1% DFM (1 wt% Ru, 6.1 wt% "Na_2O"/Al_2O_3) throughout the study.

2.2. Materials characterization

FT-IR spectra were obtained using a Nicolet Nexus Fourier Transform instrument equipped with a DTGS detector with a resolution of 4 cm^{-1} (number of scans = 20). The analysis was carried out on 15 mg of sample, crushed and compressed in a self-supporting disc of 13 mm diameter, and placed in a stainless-steel cell (ISRI Infrared Reactor, Granger, IN, USA) that allows in situ thermal treatments under vacuum or controlled atmosphere. FT-IR tests were carried out on the fresh and aged 0.5% DFM granules in order to characterize the adsorbed species at reaction conditions. Three CO_2 capture and methanation cycles were performed at 320 °C by alternating CO_2 capture (5 mbar CO_2, 10 min) and reduction (40 mbar H_2, 10 min) phases. After each phase, the sample was vacuumed for 5 min to evacuate unreacted gases. All shown spectra refer to the third cycle of capture and methanation.

In order to characterize the fresh and spent material, CO adsorption (5 mbar) was performed at 25 °C. Before all measurements, the samples were pretreated at 375 °C in H_2 (300 mbar) for 30 min.

CO pulse chemisorption tests were performed using a Thermoquest TPDRO1100 equipped with a thermal conductivity detector. CO pulses were introduced at room temperature on 100 mg of catalyst, after in situ pre-reduction (5 vol% H_2/Ar, 1 h at 500 °C, heating rate: 10 °C/min) and inert purge (30 min at 500 °C then cooled to room temperature). In all cases, 1:1.5 Ru:CO stoichiometry was assumed for the evaluation of the dispersion [15] and a hcp (hexagonal close-packed) Ru particle was assumed for the calculation of the average particle diameter, using the correlation reported in [15].

2.3. Fixed bed reactor aging studies

The tablet, ring tablet, and granule samples were aged for at least 50 cycles. In aging tablet and ring tablets, 10 g of sample was placed in a quartz packed bed reactor (O.D. = 25.8 mm, I.D. = 22 mm, L = 600 mm). The reactor tube was placed in a furnace (MTSC12.5 R x 18–1Z, Mellen, USA) with temperature feedback control from a K-type thermocouple (Omega, USA) at the middle of the DFM bed. Compressed gases were mixed at designated flow rates with mass flow controllers. Steam was delivered using a reactor feed tube pre-heated to 200 °C, which vaporized water injected by a syringe pump (Cole-Parmer, USA). An ice bath was placed at the exit of the reactor to condense the steam from the feed as well as that produced during the methanation reaction. The dry gas composition was analyzed in an Enerac 700 at NTP.

Tablet and ring tablet samples were pre-reduced in situ at 350 °C (at a heating rate of 2 °C/min) for 3 h with 20% H_2/N_2 with a total flow rate of 2 L(NTP)/h/g_{DFM} to form catalytically active Ru^0 and to hydrogenate the Na_2CO_3 precursor to "Na_2O". After pre-reduction, the reactor was cooled to 320 °C for isothermal aging cycles. Each cycle includes:

1. CO_2 capture with simulated flue gas conditions (7.5% CO_2, 4.5% O_2, 15% H_2O, N_2 balance) for 10 min at a total flow rate of 400 ml/min (Gas Hourly Space Velocity (GHSV): 1300 h^{-1})
2. N_2 purge for 4 min at a total flow rate of 400 ml/min
3. Hydrogenation with 15% H_2/N_2 for 10 min at a total flow rate of 400 ml/min.
4. N_2 purge for 4 min at a total flow rate of 400 ml/min

Steps 2 and 4 (N_2 purge) were required to avoid contact of O_2, always present in the simulated flue gas, and H_2. At least 50 consecutive CO_2 adsorption/methanation cycles were performed.

Similarly, 1 g of 0.5% DFM granules was loaded in a smaller quartz tube reactor (O.D. = 12.75 mm, I.D. = 10.5 mm, L = 500 mm) and aged in the set up described above. The granules were also pre-reduced in situ following the same procedure; after pre-reduction, the reactor was cooled to 320 °C for isothermal cycles under the same conditions detailed above, but using a total flowrate of 200 ml/min (GHSV: 7700 h^{-1}).

Following the cycles, all samples were left to cool to room temperature in N_2 and passivated using a dilute stream of O_2 (2 vol% O_2/N_2) at a flow rate of 1 L(NTP)/h/g_{DFM} before discharging the reactor to protect against over oxidation.

For comparison, a 50-cycle aging study was performed on 0.5% DFM granules using a clean stream of CO_2 during adsorption (i.e. 7.5 vol% CO_2/N_2, no O_2 or H_2O). All other conditions and cyclic durations are as detailed above. This is further denoted as "clean aging".

2.4. Fixed bed microreactor transient studies

Transient analysis of the CO_2 adsorption/reduction cycles were also performed. These experiments were performed on 120 mg of 0.5% DFM granules loaded in a quartz microreactor (internal diameter = 8 mm) connected to a gas manifold for step changes in the inlet gas concentration. The gases leaving the reactor were continuously analyzed by

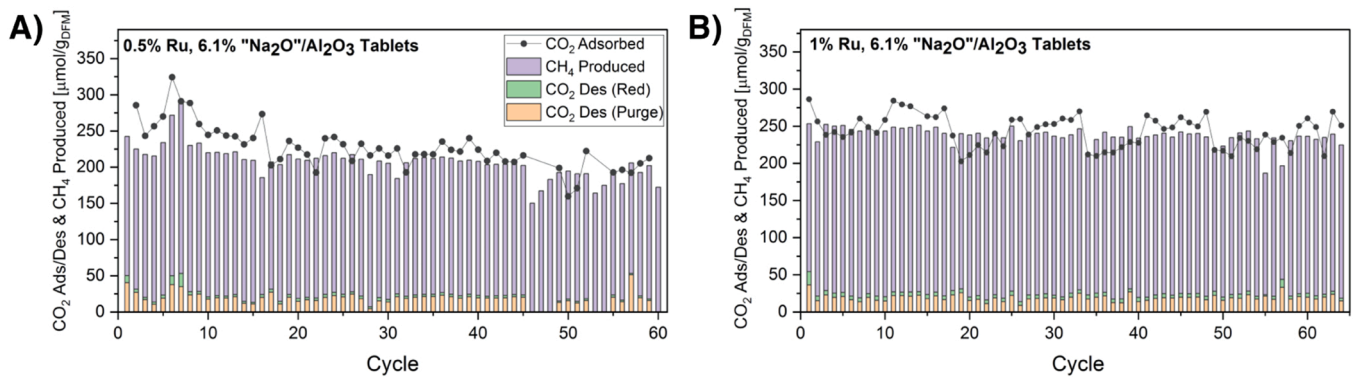

Fig. 1. CO_2 adsorption (black dots) and CH_4 production (purple bars) for 60 + cycles of adsorption/methanation on (A) 0.5% DFM tablets and (B) 1% DFM tablets. All cycles were performed at 320 °C and 1 atm; adsorption was conducted under simulated flue gas composition (7.5% CO_2, 4.5% O_2, 15% steam, balance N_2) and methanation under 15% H_2/N_2. Experimental details can be found in section 2.3.1.

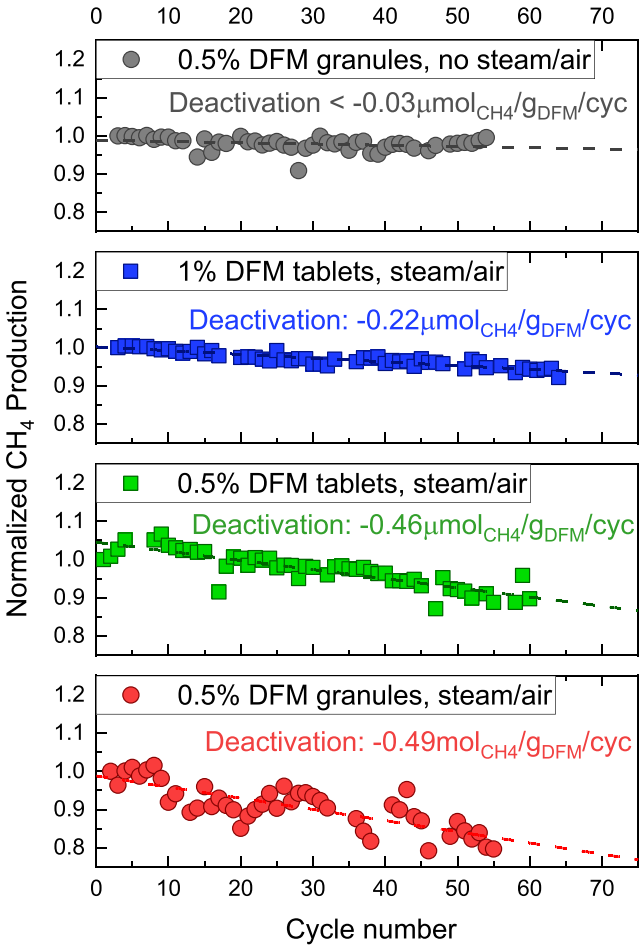

Fig. 2. Methane production results from aging on 0.5% and 1% DFMs. The reported apparent deactivation rates were evaluated by linear regression. Adsorption conditions: 7.5% CO_2, 4.5% O_2, 15% H_2O, balance N_2, 10 min. Reduction conditions: 15% H_2/N_2, 10 min. Aging was also performed without O_2 and H_2O (gray dots). All tests are performed at 320 °C and 1 atm, 1300 h^{-1} GHSV for tablets, and 7700 h^{-1} GHSV for granules.

means of a Pfeiffer QMS200 quadrupole mass spectrometer and a MKS Multigas 2030 FT-IR spectrometer. An Agilent micro gas chromatograph was also used for periodic analysis of CH_4, CO and CO_2.

Before the test, the sample was pre-treated in 4 vol% H_2/He at 500 °C with a heating rate of 10 °C/min to decompose the carbonate precursor. Cyclic experiments were performed at the constant temperature of 350 °C and with a constant flowrate of 200 ml (NTP)/min (GHSV: 60000 h^{-1}). A CO_2 capture and methanation cycle is composed by a 10 min adsorption step and a 10 min reduction step, each followed by a 5 min inert purge.

A total of 9 cycles were performed on the same sample, divided in 3 sets composed of 3 cycles each. After each set the temperature was increased in 4 vol% H_2/He to 500 °C to sweep the DFM surface. The reduction phase atmosphere was maintained equal to 4 vol% H_2/He for each cycle. On the other hand, two different adsorption atmospheres have been tested: 1 vol% CO_2/He, defined as "ideal" conditions, and 1 vol% CO_2/3 vol% O_2/2.5 vol% H_2O/He, defined as "air+steam" conditions. The first set (3 cycles) was carried out with an "ideal" adsorption atmosphere; the second set (3 cycles) with a "air+steam" adsorption atmosphere; the third set (3 cycles) with an "ideal" adsorption atmosphere.

3. Results and discussion

3.1. Fixed bed reactor aging study of low Ru loading DFM

Fixed bed, cyclic aging studies were performed on low Ru loading DFM supported on granules, tablets, and ring tablets in simulated power plant flue gas conditions (7.5 vol% CO_2, 4.5 vol% O_2, 15 vol% steam, balance N_2) to assess their stability. Cyclic quantification of CO_2 adsorption and CH_4 production of 0.5% DFM and 1% DFM tablets are shown in Fig. 1.

It is evident in Fig. 1 that for both materials, there is consistency between the CO_2 adsorbed and the amount of CH_4 produced. The data collected for CH_4 had much lower instrumental error margins due to the lower concentration, and thus the CH_4 data was more reliable to determine the rate of deactivation. Therefore, methane production during aging of all samples is shown in Fig. 2, with fitted linear regressions to determine the rates of deactivation.

Without O_2 or H_2O (gray profile) present in the adsorption step, the 0.5% DFM granules show stable and consistent methane production, indicating essentially no deactivation (< 0.03 $\mu mol_{CH4}/g_{DFM}$/cycle of loss). The results of aging 0.5% DFM tablets with simulated flue gas (with O_2 and steam; green and red profiles), however, show a clear trend of loss in CH_4 production. This comparison demonstrates that the combination of O_2 and H_2O in the feed contribute to the deactivation of the material. In particular, it is suspected that O_2 causes sintering of the catalyst species as previously shown by Bermejo-López et al. [16]. By aging Ru-NiNa and NiNa DFMs over 20 cycles with and without O_2, the authors showed that both DFMs only deactivated in the cycles with O_2. Sintering of the Ru has also been observed in this study as will be shown in Sections 3.2 and 3.3.

The 1% DFM (blue squares) exhibits a deactivation rate of 0.22

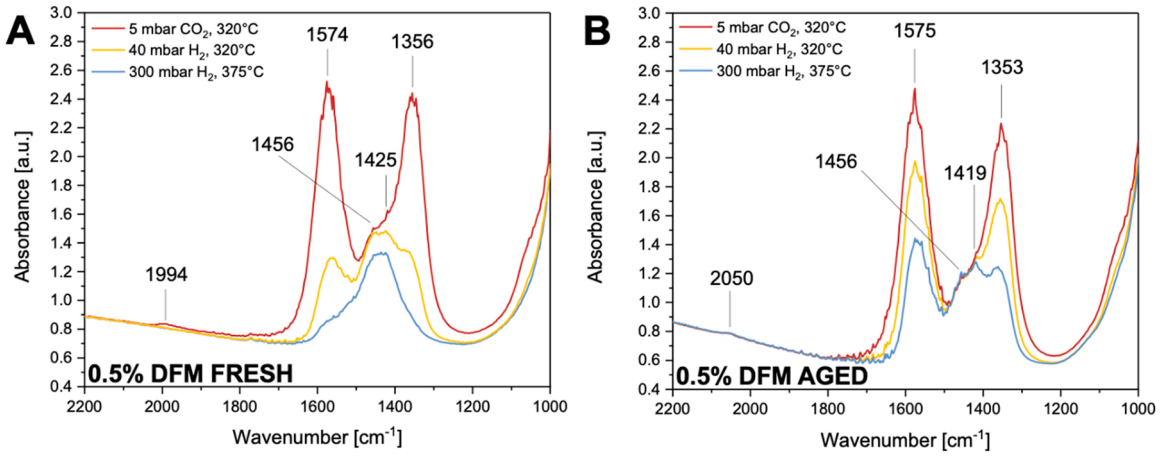

Fig. 3. FT-IR spectra recorded after 10 min of 5 mbar of CO_2 at 320 °C (red), subsequent exposure to 40 mbar H_2 at 320 °C (yellow), and subsequent exposure to 300 mbar H_2 at 375 °C (blue) on the fresh (A) and aged (B) 0.5% DFM granules. Experimental details can be found in section 2.2.2.

$\mu mol_{CH4}/g_{DFM}$/cycle when aged with adsorption in steam and air. This is half the deactivation of the 0.5% DFM tablets at the same process conditions, indicating that a higher Ru loading adds stability to the performance. This is consistent with the previous study that demonstrated stability for 5% Ru, 6.1% "Na_2O"/Al_2O_3 tableted materials in the same simulated flue gas condition [12]. Furthermore, the tested 1% DFM and 5% Ru, 6.1% "Na_2O"/Al_2O_3 DFM have the same Na_2O loading; the fact that the 5% Ru DFM showed no deactivation over 50 cycles of capture/methanation in the same simulated flue gas indicates that the main deactivating component is Ru and not Na_2O.

Three configurations were investigated for the 0.5% DFM and all exhibited a similar deactivation rate. The tablets (green squares) deactivate at a rate of 0.46 $\mu mol/g_{DFM}$/cycle and the 300 μm granules (red circles) at 0.49 $\mu mol/g_{DFM}$/cycle. Ring tablets (not reported) were also tested and these deactivate at a rate of 0.43 $\mu mol/g_{DFM}$/cycle. As all the 0.5% DFMs deactivate at essentially the same rate, it can be concluded

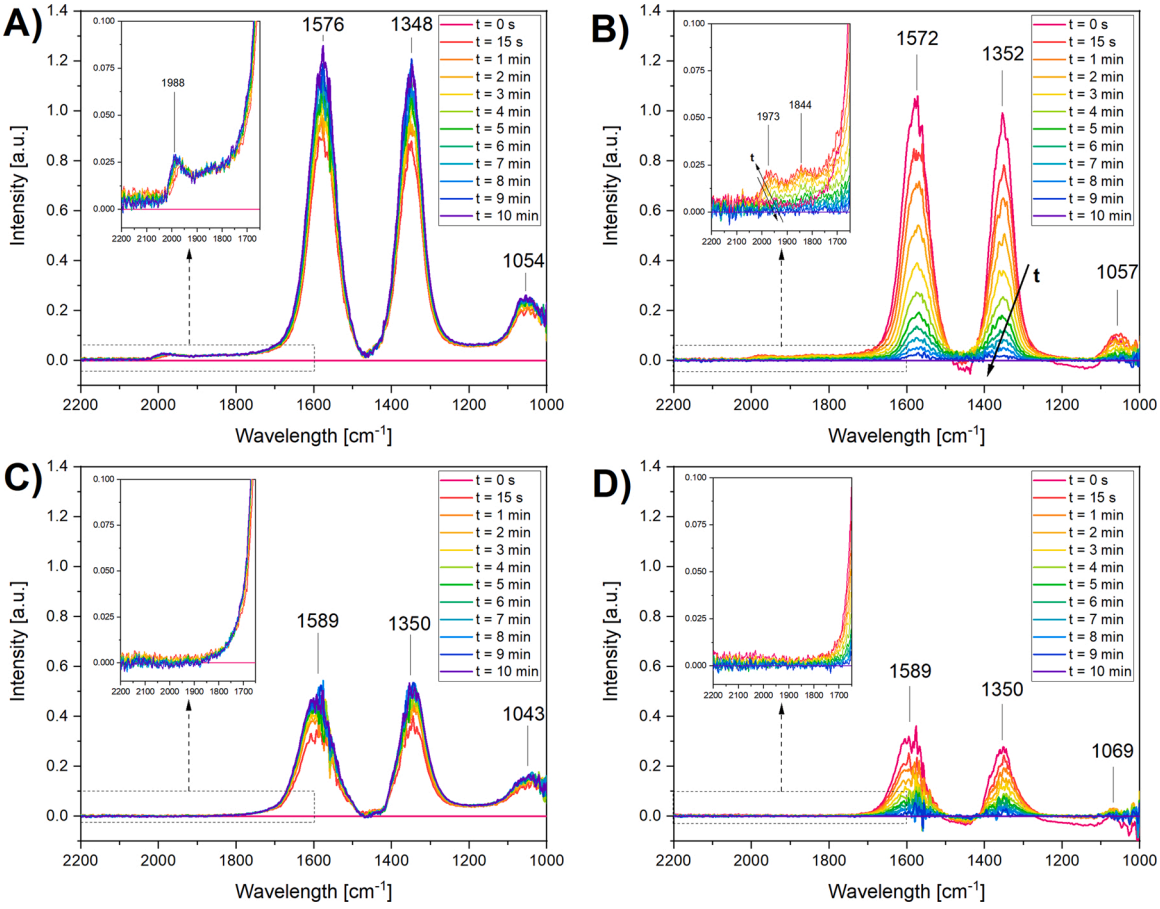

Fig. 4. FT-IR spectra during the third cycle of CO_2 capture (A) and subsequent hydrogenation (B) at 320 °C on the fresh 0.5% DFM granules. The corresponding spectra obtained during capture and hydrogenation on the aged 0.5% DFM granules are reported in panels (C) and (D), respectively. CO_2 capture conditions: 5 mbar CO_2, 10 min; hydrogenation conditions: 40 mbar H_2, 10 min. Experimental details can be found in section 2.2.2.

that the different geometries, preparation methods, and type of alumina do not contribute significantly to deactivation. Specifically, the large amounts of HNO_3 introduced in the preparation of the tablets and ring tablets do not seem to alter the catalytic activity of the material. This was also previously observed during cofeeding tests of CO_2 and H_2 [14].

3.2. FT-IR characterization of fresh and aged samples

FT-IR was used to better understand the mechanism of DFM deactivation. 0.5% DFM was studied in detail due its more severe deactivation. Fig. 3 shows spectra on fresh (A) and aged (B) DFM after exposure to adsorptive and reducing environments.

The red spectra in Fig. 3 reflect species that are present on the fresh (A) and aged (B) 0.5% DFM granules after 10 min of CO_2 adsorption at 320 °C. In both fresh and aged samples, two intense features at ~1575 and ~1355 cm^{-1} arise after CO_2 exposure, corresponding to chelating and bridged bidentate carbonates forming on Na [17–19]. The broad shoulder visible at 1420–1460 cm^{-1} is associated to the asymmetric mode of ionic carbonates on Na [19–21]. This is likely indicative of residual bulk Na_2CO_3 species from the preparation step. A contribution of bicarbonates species cannot be ruled out [22,23], but is not detected in this study. Interestingly, the total amount of bidentate carbonate formation upon CO_2 exposure is very similar between the fresh and aged sample (red spectra in Fig. 3A and B), indicating that the overall storage capacity of CO_2 is not affected by the aging process and therefore the Na_2O component is unaffected.

Upon introduction of 40 mbar of H_2 for 10 min at the same temperature of 320 °C, a substantial amount of bidentate carbonates is reduced in the fresh sample (Fig. 3A, yellow spectrum). The aged sample, however, shows only a slight reduction in the amount of bidentate carbonate species (Fig. 3B, yellow spectrum). This indicates that the aged sample is not able to reduce the surface bidentate carbonates to the same degree of the fresh sample, suggesting that some deactivation of the Ru may be occurring. It is suspected that upon aging, stronger carbonates are resistant to hydrogenation due to lower methanating ability of the Ru.

Subsequently, both samples were also treated with 300 mbar of H_2 for 1 h at 375 °C (blue spectra). On the fresh sample (Fig. 3A), the bands corresponding to bidentate carbonates are essentially undetectable, while the band of monodentate/bulk sodium carbonates remains evident. This indicates that these carbonates species are more difficult to hydrogenate, in agreement with previous observations in similar conditions reported by some of us in the case of carbonates formed on Ba upon CO_2 exposure [19]. On the aged sample (Fig. 3B) the bands of bidentate carbonates are still clearly present even after conditioning in a more favorable reducing environment (high H_2 partial pressure and high temperature). In addition, the band corresponding to monodentate/bulk carbonates remains almost unchanged. This clearly points at a lower hydrogenating ability of the aged sample, considering that no significant differences in the nature of the adsorbed species was evidenced by FT-IR. This is also consistent with a reduced activity of aged Ru.

Fig. 4 shows the results of the FT-IR characterization during CO_2 capture and reduction in H_2 at 320 °C on the fresh and aged 0.5% DFM granules. In this case, to appreciate better the spectral features and to compare the net amount of surface carbonates adsorbed and reduced in each cycle, the spectra are the result of a subtraction, using as subtrahend the corresponding spectrum obtained at the end of the hydrogenation phase (i.e., yellow spectra shown in Fig. 3).

When the fresh sample is exposed to CO_2, three intense bands at 1576, 1348 and 1054 cm^{-1} grow rapidly in the first 15 s of exposure (Fig. 4A). These features are associated with surface carbonates formed on Na. In addition, a small and broad spectral feature appears in the range 2050–1800 cm^{-1}, with a maximum at ~1990 cm^{-1}. This is associated with the presence of carbonyl species in multiple configurations on Ru sites in multiple oxidation states [24], likely as a result of the reaction of CO_2 with residual H_2 from the hydrogenation phase of the previous cycle [25,26].

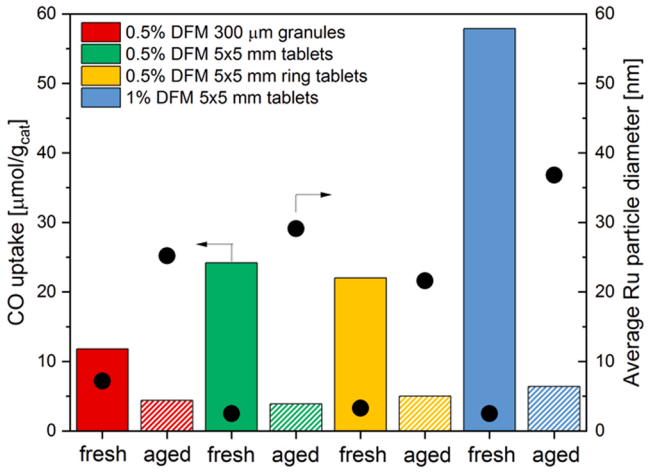

Fig. 5. CO uptake (bars) and corresponding average Ru particle size (dots) evaluated from pulse chemisorption at room temperature on fresh DFMs (solid) and aged DFM (hatched). Experimental details can be found in section 2.2.3.

During the vacuum purge (not shown) between the adsorption and the hydrogenation step, only minor amounts of Na-carbonates are removed from the catalyst surface, while Ru-carbonyls are completely removed (compare the spectra at t = 10 min in Fig. 4A with the spectra at t = 0 s in Fig. 4B).

The bands associated with carbonates on Na decrease upon H_2 admission at 320 °C, with a 60% reduction of band intensity in the first 2 min of H_2 exposure. While the carbonates monotonically decrease with time, carbonyls on Ru rapidly increase to reach their maximum intensity after 1 min of H_2 exposure. This band progressively decreases until t = 5 min, after which it is no longer detected. This is well in line with the role of adsorbed CO as intermediate product in the CO_2 methanation reaction [27,28].

Fig. 4 C and D show the results of the FT-IR characterization during CO_2 capture and subsequent reduction in H_2 at 320 °C on the aged 0.5% DFM granules. When the aged sample is exposed to CO_2 (Fig. 4C), bidentate carbonate bands are formed with the same dynamic discussed in the case of the fresh sample, but with much lower intensity. This indicates that the total amount of carbonate species on the aged DFM is comparable to the fresh sample (as discussed with Fig. 3), but the amount of carbonates formed per cycle (i.e. the amount of CO_2 adsorbed per cycle) is much lower in the case of the aged DFM. Interestingly, those bands of carbonyls species on Ru are not detected during the adsorption step, and during the reduction step. This agrees well with the lower hydrogenation activity of the aged sample.

3.3. CO chemisorption on fresh and aged samples

CO pulse chemisorption are carried out on fresh and aged DFMs to characterize the active Ru sites. The results are reported in Fig. 5 in terms of CO uptake and average Ru crystallite size. The average particle diameter was calculated for each sample from the total CO chemisorbed and by assuming the nominal Ru loading for each sample.

The amount of CO chemisorbed is consistently lower for the aged samples compared to the corresponding fresh samples (compare solid bars with hatched bars). This indicates that there is less active Ru surface area available for CO adsorption, which is consistent with the decrease in CH_4 formation during aging (Fig. 2). This points to three possible modes of deactivation when the material is aged in the presence of steam and O_2 in the capture step: Ru sintering, RuO_x volatilization, or Ru masking due to mobilization of the sodium species.

While it is possible that some of the available Ru is oxidized to bulk RuO_x (particularly RuO_2) at DFM operating temperatures (320–350 °C),

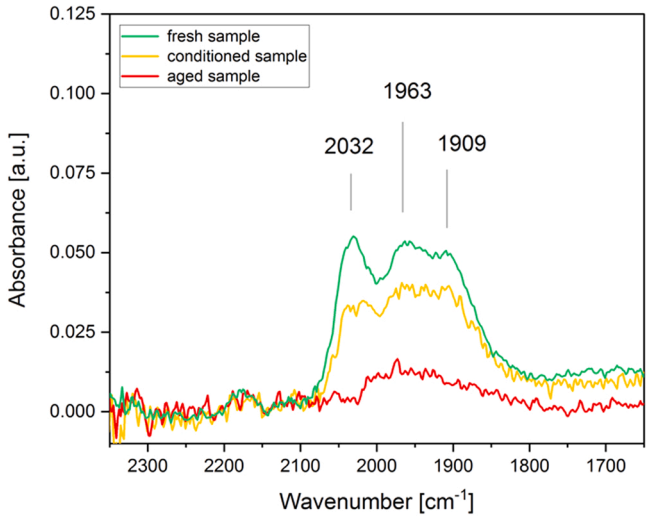

Fig. 6. FT-IR spectra recorded after 20 min of 5 mbar of CO exposure on the fresh (green), conditioned (yellow) and aged (red) 0.5% DFM granules. Experimental details can be found in section 2.2.2.

volatilization of the oxidized species is not feasible [29,30]. When studying Ru/Na-Y as a catalyst for CO oxidation, Villani et al. found indeed that even after treating their catalyst in dry air at 500 °C, there was no loss in total Ru content. In addition, TGA studies showed that loss of Ru by volatilization only occurred at temperatures above 900 °C [29]. We also suspect that Na_2O migration leading to Ru masking is not the primary mode of deactivation. Na_2O could in fact be mobilized due to the presence of moisture in the simulated flue gas conditions; however, in this case, we would have expected to see this effect to a milder extent even in the no steam/air aging tests. In those tests, moisture would be present as a product of methanation, but we have not observed any meaningful signs of deactivation of the DFM (gray profile in Fig. 2). Furthermore, FT-IR tests during CO_2 adsorption on the fresh and aged 0.5% DFM (shown in Fig. 3) did not indicate any meaningful differences in neither the type of adsorbed species nor in their amount, suggesting the absence of significant changes in Na morphology upon aging. This leaves sintering of the Ru to be main suspected mode of deactivation.

Of the fresh samples, the 0.5% DFM granules exhibit the lowest CO uptake (11.8 μmol/g_{DFM}), corresponding to a Ru^0 average particle diameter of 7 nm. This is consistent with the methane production results seen in Fig. 2, where the 0.5% DFM showed lower methane production than the tablet and ring tablet 0.5% DFMs. Accordingly, the 0.5% DFM tablets and ring tablets show higher CO uptake (24.2 and 22.0 μmol/g_{DFM}, respectively). The 1% DFM shows the highest CO uptake (57.9 μmol/g_{DFM}), correlating to the highest methane production as seen in Fig. 2. These values are well in line with those measured by H_2 chemisorption on γ-Al_2O_3 pellets sharing the same preparation method [31].

All aged samples exhibit much lower CO uptake values (consistently below 10 μmol/g_{DFM}) and larger average particle sizes (in all cases larger than 20 nm) with respect to their corresponding fresh samples, indicating that there is loss in Ru active sites most likely due to sintering. Further evidence of Ru sintering is shown by FT-IR analysis during CO adsorption in Fig. 6.

The fresh sample (green) shows a complex envelope, with three main bands at 2032,1963 and 1909 cm^{-1}. The band at 2032 cm^{-1} can be assigned to linearly bonded CO [22,24]. The bands at the lower frequencies are of more complex attribution, and are usually assigned to bridged carbonyls, di-carbonyls, or three-fold carbonyl species on Ru sites in different oxidation states [24,27,32–34]. CO adsorption at room temperature was performed on a "conditioned" sample (yellow spectra) which was exposed in the to three cycles of capture/methanation at

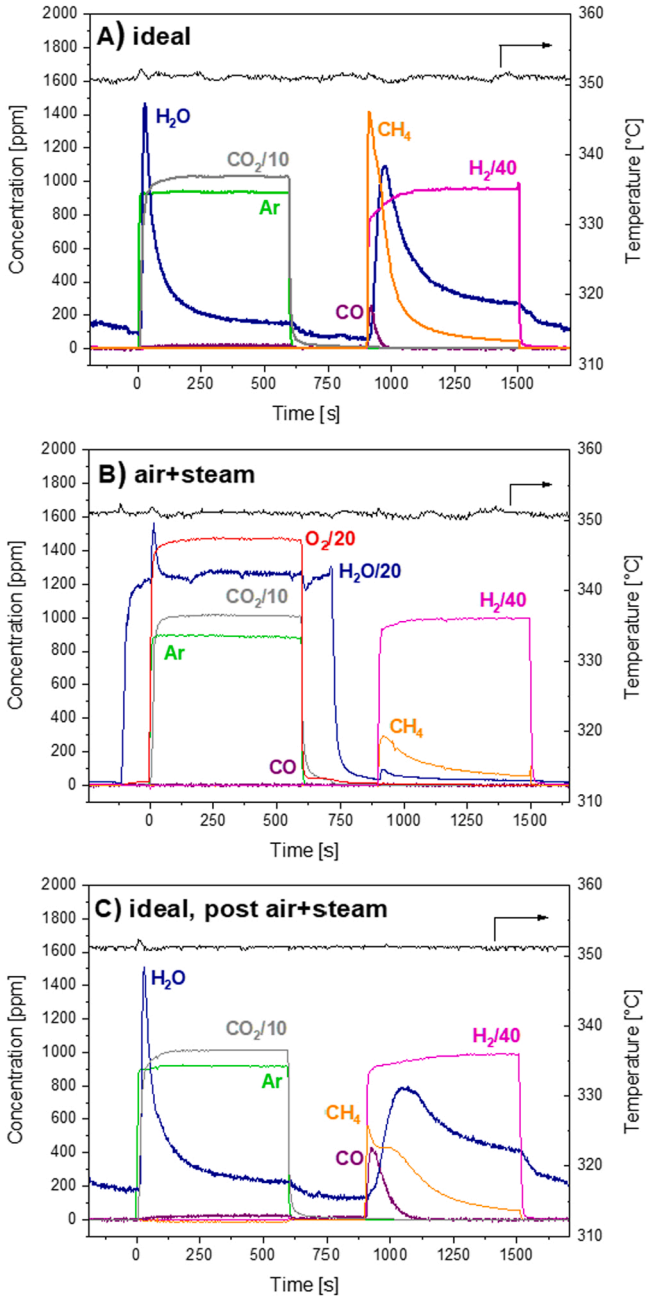

Fig. 7. Cycles of sequential CO_2 capture and methanation on fresh 0.5% DFM granules with different adsorption conditions: (A) 1% CO_2/He over a fresh catalyst sample (ideal, 3rd cycle), (B) 1% CO_2/ 3% O_2/ 2.5% H_2O /He (air-+steam, 6th cycle), (C) 1% CO_2/He (ideal, 9th cycle). Reduction conditions: 4% H_2/He. The gas measurements at the reactor outlet have been scaled to fit in a single graph (for example, CO_2/10 indicates that an outlet value of 1% was divided by 10 to be plotted as 1000 ppm in the figure). Experimental details can be found in Section 3.4.

350 °C (capture conditions: CO_2 5 mbar, O_2 30 mbar, 10 min; reduction conditions: H_2 40 mbar, 10 min). This sample shows the same Ru-carbonyl bands observed on the fresh sample but with lower intensity, possibly indicating a decrease in the available Ru sites. CO adsorption at room temperature on the spent sample after the aging test reported in Fig. 2 (red spectra) resulted in a much lower and broader band, corresponding to the lowest absorbance in agreement with the CO chemisorption results reported in Fig. 5. In addition to the lower intensity, the band corresponding to linearly bonded CO disappears, leaving only the broad band at ~1970 cm^{-1}.

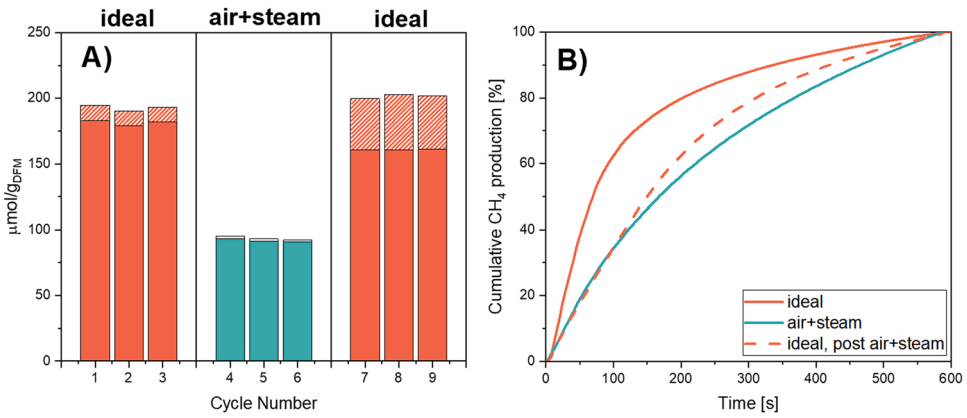

Fig. 8. (A) Quantitative results in terms of amount of CH_4 (solid) and CO (hatched) formed during the reduction step during sequential cycles in the conditions reported in Fig. 7; (B) Cumulative integral CH_4 formation during the three cycles shown in Fig. 7.

3.4. Fixed bed microreactor transient study of low Ru loading DFM

Three sets of cycles were performed on fresh 0.5% DFM granules, as detailed in the experimental section, to investigate the dynamics of the CO_2 adsorption/reduction steps and the effect of the O_2 and steam presence during the adsorption feed on the catalyst transient behavior. The last cycle of each set is reported in Fig. 7.

Fig. 7A refers to the "ideal" condition (i.e., cycles carried out in the absence of water and oxygen in the feed during the CO_2 capture step). Upon CO_2 admission, a sharp H_2O peak is observed. This likely arises from the CO_2 adsorption on a hydrated sodium oxide species, which forms a carbonated sodium species and water [35]. The concentration of CO_2 in the gas phase reaches the inlet value of 1% after 2 min of adsorption, indicating the quick saturation of the sample with CO_2 ad-species. These results are in good agreement with FT-IR results shown in Fig. 6A.

When H_2 is admitted, a sharp CH_4 peak is produced along with water, that is tailing due to its adsorption on the surface. A lower peak of CO is also detected, likely as the result of incomplete CO_2 reduction occurring via reverse water gas shift reaction. The integrated amounts of CH_4 and CO produced during the cycles are shown in Fig. 8 A.

Fig. 7B shows a cycle carried out in the presence of 3 vol% O_2 and 2.5 vol% H_2O during the CO_2 capture step. Focusing on the reduction step, it appears that the presence of water and oxygen during the adsorption step results in a lower methane production once the carbonated DFM is exposed to H_2 (see also Fig. 8 A). Interestingly, the CO formation observed under the "ideal" conditions is completely suppressed.

Finally, ideal cycles were run on the same DFM after O_2/H_2O cycles (Fig. 7 C). By comparing Fig. 7 A and C, it can be observed that the adsorption step is very similar, with comparable amounts of CO_2 adsorbed (and H_2O released). On the other hand, the evolution of CH_4 and CO during the reduction step appears quite different. Indeed, the CH_4 (and H_2O) peak is broader upon hydrogenation after cycles in the presence of O_2/H_2O (Fig. 7 C), indicating a lower rate of CH_4 formation. Also, the production of CO (seen at the beginning of the hydrogenation phase) appears enhanced. Yet, the overall amounts of CH_4 + CO evolved is similar to the ideal case on the fresh sample (Fig. 8 A).

The normalized cumulative integral of CH_4 formation as a function of time for the three cases shown in Fig. 7 are reported in Fig. 8B. In this graph, the slope of each curve is proportional to the rate of CH_4 formation, regardless of the total amount of methane produced.

In the presence of O_2/H_2O during the capture step, the amount of methane produced is nearly half that of the fresh sample during ideal cycles (compare red and blue bars in Fig. 8 A). Furthermore, the rate of methane formation is slower after capture in the presence of O_2/H_2O (Fig. 8B), as indicated by the milder slope of the cumulative methane formation at the beginning of the reduction step (compare solid red and blue lines).

When ideal cycles are performed again after O_2/H_2O cycles, the amount of CH_4 formed during the reduction step is 12% lower than that formed in the same conditions on the fresh DFM. An opposite trend is observed in the case of CO, as higher amounts are detected after O_2 and H_2O exposure. Additionally, the rate of CH_4 production appears compromised after cycles in the presence of O_2 and H_2O as the cumulative CH_4 production retains the same initial lower slope observed during O_2/H_2O cycles. However, as already pointed out, it is noteworthy that the total amount of C product ($CO+CH_4$) is comparable in both cases (before and after O_2/H_2O exposure).

These results indicate that O_2/H_2O exposure irreversibly affects the performance of the DFM. In fact, while the amount of captured CO_2 as well as the amount of C-containing reduction products remains comparable before and after O_2/H_2O cycles, the conversion of the adsorbed CO_2 into CH_4 occurs with a lower rate and selectivity. This is consistent with a reduction in the activity of the catalyst induced by a decrease of the Ru active area of the DFM due to sintering.

4. Conclusions

Due to economic concerns of high Ru loading DFM, aging studies for a simulated power plant flue gas (7.5% CO_2, 4.5% O_2, 15% steam, balance N_2) were conducted to evaluate the stability of 0.5 wt% and 1 wt% Ru DFM. At least 50 cycles of CO_2 adsorption from simulated flue gas and subsequent methanation were carried out on about 10 g of DFMs. Very slight but steady deactivation was observed in all cases when the adsorption feed was the simulated flue gas containing O_2 and H_2O at 320 °C. The deactivation rate seems unaffected by the morphology of the support and by the preparation method but is more severe as the Ru loading decreases. It is suspected that O_2/H_2O contribute to Ru deactivation as stable performance was observed when the adsorption feed was free of O_2 and steam. Deactivation of Ru after exposure to O_2/H_2O was confirmed by in situ FT-IR studies and CO chemisorption, which show that the aged DFM samples have less available active Ru surface area and thus, lower methanating ability. A closer investigation into the dynamics of adsorption and methanation shows after O_2/H_2O exposure, the DFM performance is irreversibly affected due to Ru sintering, resulting in lower methanation rate and lower selectivity towards methane.

CRediT authorship contribution statement

Chae Jeong-Potter: Writing – original draft, Conceptualization, Methodology, Validation, Investigation, Visualization, Formal analysis. **Alessandro Porta.** Writing – original draft, Conceptualization,

Methodology, Validation, Investigation, Visualization, Formal analysis. **Roberto Matarrese.** Writing – review & editing, Methodology. **Carlo Giorgio Visconti.** Writing – review & editing, Funding acquisition. **Luca Lietti.** Writing – review & editing, Supervision, Project administration, Funding acquisition. **Robert J. Farrauto.** Writing – review & editing, Supervision, Project administration, Funding acquisition.

Declaration of Competing Interest

The authors declare that they have no known competing financial interests or personal relationships that could have appeared to influence the work reported in this paper.

Acknowledgements

The authors would like to thank the Cohn Memorial Fellowship and Anglo American, UK for their financial support. Our gratitude extends to SASOL, Germany for providing a variety of Al2O3 samples for testing.

References

[1] E. Dlugokencky, P. Tans, Trends in Atmospheric Carbon Dioxide, Www.Esrl.Noaa.Gov/Gmd/Ccgg/Trends/. (2020).
[2] IEA, World Energy Outlook 2017, OECD Publishing, Paris, 2017, https://doi.org/10.1787/weo-2017-en.
[3] P. Melo Bravo, D.P. Debecker, Combining CO_2 capture and catalytic conversion to methane, Waste Dispos. Sustain. Energy 1 (2019) 53–65, https://doi.org/10.1007/s42768-019-00004-0.
[4] R.J. Farrauto, M.S. Duyar, A.A. Park, Methods, systems and materials for capturing carbon dioxide and converting it to a chemical product, WO 2016/007825 A1, 2016.
[5] I.S. Omodolor, H.O. Otor, J.A. Andonegui, B.J. Allen, A.C. Alba-Rubio, Dual-function materials for CO_2 capture and conversion: a review, Ind. Eng. Chem. Res. 59 (2020) 17612–17631, https://doi.org/10.1021/acs.iecr.0c02218.
[6] M.S. Duyar, S. Wang, M.A. Arellano-treviño, R.J. Farrauto, CO_2 utilization with a novel dual function material (DFM) for capture and catalytic conversion to synthetic natural gas: an update, J. CO2 Util. 15 (2016) 65–71, https://doi.org/10.1016/j.jcou.2016.05.003.
[7] M.A. Arellano-Treviño, Z. He, M.C. Libby, R.J. Farrauto, Catalysts and adsorbents for CO_2 capture and conversion with dual function materials: limitations of Ni-containing DFMs for flue gas applications, J. CO2 Util. 31 (2019) 143–151, https://doi.org/10.1016/j.jcou.2019.03.009.
[8] C. Janke, M.S. Duyar, M. Hoskins, R.J. Farrauto, Catalytic and adsorption studies for the hydrogenation of CO_2 to methane, Appl. Catal. B: Environ. 152–153 (2014) 184–191, https://doi.org/10.1016/j.apcatb.2014.01.016.
[9] M.S. Duyar, M.A. Arellano, R.J. Farrauto, Dual function materials for CO_2 capture and conversion using renewable H_2, Appl. Catal. B: Environ. 168 (2015) 370–376, https://doi.org/10.1016/j.apcatb.2014.12.025.
[10] Q. Zheng, R.J. Farrauto, A. Chau Nguyen, Adsorption and methanation of flue gas CO_2 with dual functional catalytic materials: a parametric study, Ind. Eng. Chem. Res. 55 (2016) 6768–6776, https://doi.org/10.1021/acs.iecr.6b01275.
[11] S. Wang, E.T. Schrunk, H. Mahajan, R.J. Farrauto, The role of ruthenium in CO_2 capture and catalytic conversion to fuel by dual function materials (DFM), Catalysts 7 (2017) 88, https://doi.org/10.3390/catal7030088.
[12] S. Wang, R.J. Farrauto, S. Karp, J.H. Jeon, E.T. Schrunk, Parametric, cyclic aging and characterization studies for CO_2 capture from flue gas and catalytic conversion to synthetic natural gas using a dual functional material (DFM), J. CO2 Util. 27 (2018) 390–397, https://doi.org/10.1016/j.jcou.2018.08.012.
[13] M.A. Arellano-treviño, N. Kanani, C.W. Jeong-potter, R.J. Farrauto, Bimetallic catalysts for CO_2 capture and hydrogenation at simulated flue gas conditions, Chem. Eng. J. 375 (2019), 121953, https://doi.org/10.1016/j.cej.2019.121953.
[14] A. Porta, L. Falbo, C.G. Visconti, L. Lietti, C. Bassano, P. Deiana, Synthesis of Ru-based catalysts for CO_2 methanation and experimental assessment of intraporous transport limitations, Catal. Today (2019) 0–1, https://doi.org/10.1016/j.cattod.2019.01.042.
[15] A. Comas-Vives, K. Furman, D. Gajan, M.C. Akatay, A. Lesage, F.H. Ribeiro, C. Copéret, Predictive morphology, stoichiometry and structure of surface species in supported Ru nanoparticles under H_2 and CO atmospheres from combined experimental and DFT studies, Phys. Chem. Chem. Phys. 18 (2016) 1969–1979, https://doi.org/10.1039/c5cp06710c.
[16] A. Bermejo-López, B. Pereda-Ayo, J.A. González-Marcos, J.R. González-Velasco, Alternate cycles of CO_2 storage and in situ hydrogenation to CH_4 on Ni-Na_2CO_3/Al_2O_3: influence of promoter addition and calcination temperature, Sustain. Energy Fuels 5 (2021) 1194–1210, https://doi.org/10.1039/d0se01677b.
[17] F. Prinetto, M. Manzoli, S. Morandi, F. Frola, G. Ghiotti, L. Castoldi, L. Lietti, P. Forzatti, Pt−K/Al_2O_3 NSR catalysts: characterization of morphological, structural and surface properties, J. Phys. Chem. C. 114 (2010) 1127–1138, https://doi.org/10.1021/jp909026p.
[18] L. Proaño, M.A. Arellano-Treviño, R.J. Farrauto, M. Figueredo, C. Jeong-Potter, M. Cobo, Mechanistic assessment of dual function materials, composed of Ru-Ni, Na_2O/Al_2O_3 and Pt-Ni, Na_2O/Al_2O_3, for CO_2 capture and methanation by in-situ DRIFTS, Appl. Surf. Sci. 533 (2020), 147469, https://doi.org/10.1016/j.apsusc.2020.147469.
[19] A. Porta, R. Matarrese, C.G. Visconti, L. Castoldi, L. Lietti, Storage material effects on the performance of Ru-based CO 2 capture and methanation dual functioning materials, Ind. Eng. Chem. Res. 60 (2021) 6706–6718, https://doi.org/10.1021/acs.iecr.0c05898.
[20] S. Morandi, F. Prinetto, G. Ghiotti, L. Castoldi, L. Lietti, P. Forzatti, M. Daturi, V. Blasin-Aubé, The influence of CO_2 and H_2O on the storage properties of Pt-Ba/Al_2O_3 LNT catalyst studied by FT-IR spectroscopy and transient microreactor experiments, Catal. Today 231 (2014) 116–124, https://doi.org/10.1016/j.cattod.2013.12.036.
[21] Y. Qiao, J. Wang, Y. Zhang, W. Gao, T. Harada, L. Huang, T.A. Hatton, Q. Wang, Alkali nitrates molten salt modified commercial MgO for intermediate-temperature CO_2 capture: optimization of the Li/Na/K ratio, Ind. Eng. Chem. Res. 56 (2017) 1509–1517, https://doi.org/10.1021/acs.iecr.6b04793.
[22] L. Proaño, E. Tello, M.A. Arellano-Trevino, S. Wang, M. Cobo, R.J. Farrauto, In-situ DRIFTS study of two-step CO_2 capture and catalytic methanation over Ru,"Na_2O"/Al_2O_3 dual functional material, Appl. Surf. Sci. 479 (2019) 25–30, https://doi.org/10.1016/j.apsusc.2019.01.281.
[23] J. Zheng, C. Wang, W. Chu, Y. Zhou, K. Köhler, CO_2 methanation over supported Ru/Al_2O_3 catalysts: mechanistic studies by in situ infrared spectroscopy, ChemistrySelect 1 (2016) 3197–3203, https://doi.org/10.1002/slct.201600651.
[24] S.Y. Chin, C.T. Williams, M.D. Amiridis, FTIR studies of CO adsorption on Al_2O_3- and SiO_2-supported Ru catalysts, J. Phys. Chem. B 110 (2006) 871–882, https://doi.org/10.1021/jp053908q.
[25] A. Bermejo-López, B. Pereda-Ayo, J.A. González-Marcos, J.R. González-Velasco, Ni loading effects on dual function materials for capture and in-situ conversion of CO_2 to CH_2 using CaO or Na_2CO_3, J. CO2 Util. (2019), https://doi.org/10.1016/j.jcou.2019.08.011.
[26] A. Porta, C.G. Visconti, L. Castoldi, R. Matarrese, C. Jeong-Potter, R. Farrauto, L. Lietti, Ru-Ba synergistic effect in dual functioning materials for cyclic CO_2 capture and methanation, Appl. Catal. B: Environ. 283 (2021), 119654, https://doi.org/10.1016/j.apcatb.2020.119654.
[27] L. Falbo, C.G. Visconti, L. Lietti, J. Szanyi, The effect of CO on CO_2 methanation over Ru/Al_2O_3 catalysts: a combined steady-state reactivity and transient DRIFT spectroscopy study, Appl. Catal. B: Environ. 256 (2019), https://doi.org/10.1016/j.apcatb.2019.117791.
[28] I. Md, R. Alam, G. Cheula, L. Moroni, M. Nardi, Maestri, Mechanistic and multiscale aspects of thermo-catalytic CO_2 conversion to C1 products, Catal. Sci. Technol. 11 (2021) 6601–6629, https://doi.org/10.1039/d1cy00922b.
[29] K. Villani, C.E.A. Kirschhock, D. Liang, G. van Tendeloo, J.A. Martens, Catalytic carbon oxidation over ruthenium-based catalysts, Angew. Chem. - Int. Ed. 45 (2006) 3106–3109, https://doi.org/10.1002/anie.200503799.
[30] F. Garisto, Thermodynamic behaviour of ruthenium at high temperatures, AECL-9552, White Nucl. Res. Establ. (1988).
[31] A. Porta, L. Falbo, C.G. Visconti, L. Lietti, C. Bassano, P. Deiana, Synthesis of Ru-based catalysts for CO_2 methanation and experimental assessment of intraporous transport limitations, Catal. Today 343 (2020) 38–47, https://doi.org/10.1016/j.cattod.2019.01.042.
[32] M. Nawdali, H. Ahlafi, G.M. Pajonk, D. Bianchi, Elementary steps involved in the hydrogenation of the linear CO species adsorbed on a Ru/Al_2O_3 catalyst, J. Mol. Catal. A: Chem. 162 (2000) 247–256, https://doi.org/10.1016/S1381-1169(00)00293-4.
[33] P. Dongapure, S. Bagchi, S. Mayadevi, R.N. Devi, Variations in activity of Ru/TiO_2 and Ru/Al_2O_3 catalysts for CO_2 hydrogenation: an investigation by in-situ infrared spectroscopy studies, Mol. Catal. 482 (2020), 110700, https://doi.org/10.1016/j.mcat.2019.110700.
[34] S. Chen, A.M. Abdel-Mageed, M. Dyballa, M. Parlinska-Wojtan, J. Bansmann, S. Pollastri, L. Olivi, G. Aquilanti, R.J. Behm, Raising the COx methanation activity of a Ru/γ-Al_2O_3 catalyst by activated modification of metal–support interactions, Angew. Chem. Int. Ed. 59 (2020) 22763–22770, https://doi.org/10.1002/anie.202007228.
[35] A. Bermejo-López, B. Pereda-Ayo, J.A. González-Marcos, J.R. González-Velasco, Mechanism of the CO_2 storage and in situ hydrogenation to CH_2. Temperature and adsorbent loading effects over Ru-CaO/Al_2O_3 and Ru-Na_2CO_3/Al_2O_3 catalysts, Appl. Catal. B: Environ. 256 (2019), https://doi.org/10.1016/j.apcatb.2019.117845.